Lithuanian Journal of Physics, Vol. **50**, No. 4, pp. 377–394 (2010) doi:10.3952/lithjphys.50405

Review

QUASICLASSICAL THEORY OF QUANTUM DOTS

E. Anisimovas [a] and A. Matulis [b]

[a] *Department of Theoretical Physics, Vilnius University, Saulėtekio 9, LT-10222 Vilnius, Lithuania*
E-mail: egidijus.anisimovas@ff.vu.lt
[b] *Semiconductor Physics Institute, Center for Physical Sciences and Technology, A. Goštauto 11, LT-01108 Vilnius, Lithuania*
E-mail: amatulis@takas.lt

Received 30 November 2010; accepted 15 December 2010

We review the quasiclassical theory of quantum dots. The starting point of the developed approximate approaches is the observation that in large (in comparison to the effective Bohr radius) quantum dots the energy of the classical Coulomb interactions dominates over the quantum-mechanical kinetic energy. This dominance is further enhanced by application of a perpendicular magnetic field. The classical regime is marked by the formation of structures (the Wigner crystal) and structural transitions. The nature of these phenomena is indeed classical, and they can be successfully tackled using classical approaches which are transparent and easy to understand. In this way heavy calculations typical of quantum-mechanical schemes are avoided and the quantum effects are included in an perturbative manner. We discus, in particular, the application of the renormalized perturbation series to the energy spectra, the structural transitions, the power law behaviour of the critical fields, the global (persistent) and local currents in quantum dots, and dissipation in mixed systems with both quantum and classical degerees of freedom.

Keywords: quantum dots, quasiclassical approximation, Wigner crystal

PACS: 73.21.La, 03.65.Sq

1. Introduction

Quantum dots [1, 2] are man-made nanostructures where the motion of charge carriers is confined in all three spatial dimensions, and the confinement manifests itself in a discrete energy level spectrum. In this respect, quantum dots resemble atoms and, unsurprisingly, have been nicknamed *artificial atoms* [2]. Quantum dots are produced in a lab and thus – in stark contrast to the natural atoms – have tunable parameters, which make them attractive objects for fundamental studies as well as applications [3].

As far as applications and mass-production is concerned, the most convenient are the so-called *self-assembled* quantum dots [4, 5]. They can be produced in large quantities, and often come out nicely arranged in regular arrays [4, 6] by simply growing layers of two lattice-mismatched materials (a common pair is GaAs and InAs) on top of each other. These quantum dots are small objects with typical radii around 10 nm or less. Thus, the self-assembled quantum dots are most closely related to the natural atoms as the charge carrier confinement length is comparable to the effective Bohr radius of the host material, which is also approximately 10 nm for the gallium arsenide.

On the other hand, early attempts to fabricate confined pools of electrons typically employed application of electrostatic potentials to patterned gates placed above a two-dimensional electron layer [7, 8]. Quantum dots defined in this way are commonly known as electrostatic (gated), or parabolic. The latter term reflects the fact that almost any potential distribution can be reasonably well approximated by a parabola in the vicinity of its minimum point. Thus, we use the following form of the confinement potential:

$$V_{\mathrm{conf}}(r) = \frac{m^*\omega_0^2 r^2}{2}\,, \tag{1}$$

with m^* representing the electron effective mass and ω_0 defining the confinement frequency. This frequency is the oscillation frequency of either a single particle or the centre-of-mass mode of a many-particle system. The parabolic quantum dots are also significantly larger. Here, the confinement length can exceed the effective Bohr radius up to ten times. We define the confinement length as the characteristic extension of the ground-state wavefunction of a single particle

$$l_0 = \sqrt{\frac{\hbar}{m^*\omega_0}}\,. \tag{2}$$

ISSN 1648-8504

As a consequence of the size, the relative strength of the interparticle interactions is also much larger. Elementary dimensional analysis shows that the kinetic energy of a confined electron is of the order of $\hbar^2/m^*l_0^2$. The typical energy of the interparticle Coulomb interaction is $e^2/\epsilon l_0$, where ϵ denotes the dielectric constant of the medium. Thus, the relative importance of interactions can be estimated as the ratio of the characteristic energies

$$\lambda = \frac{e^2 m^* l_0}{\epsilon\hbar^2} = \frac{l_0}{a_{\rm B}^*} \quad \text{with} \quad a_{\rm B}^* = \frac{\epsilon\hbar^2}{m^* e^2}\,, \qquad (3)$$

which is equal to the ratio of the confinement length and the effective Bohr radius $a_{\rm B}^*$.

The length scales characterizing natural atoms are *fixed* and the coupling strength λ defined in an analogous fashion turns out to be of the order of unity. This implies that interactions are not particularly strong. The dimensions of quantum dots fabricated in a lab can be tuned to some extent, thereby tuning also the ratio of the defining energy scales. Even greater possibilities of control are offered by the application of a perpendicular magnetic field, which influences the interaction parameter according to

$$\lambda \to \lambda_{\rm eff} \sim \lambda\sqrt{\gamma}\,. \qquad (4)$$

Here γ is the dimensionless magnetic field strength, defined as the ratio of the cyclotron frequency $\omega_c = eB/m^*c$ to the confinement frequency ω_0:

$$\gamma = \frac{\omega_c}{\omega_0}\,. \qquad (5)$$

In general, strong interactions are known to facilitate the emergence of cooperative phenomena. Since these interactions are also tunable, the parabolic quantum dots have been recognized as an ideal laboratory to study the collective effects brought about by the strong Coulomb repulsion between the confined electrons. This has been a central topic of our studies of quantum nanostructures. Therefore, the present review mostly focuses on the physics of parabolic – that is, large and strongly correlated – quantum dots and collective phenomena.

Early reports emphasizing the observation of discreet electronic states in artificial semiconductor structures started appearing more than 20 years ago. The discreet nature of the electron energy spectrum was convincingly demonstrated using the resonant tunnelling [9], capacitance [10] and optical (far-infrared) spectroscopies [11]. Already in these pioneering studies physicists were quick to recognize the advantages offered by the ability to localize a small and controllable number of particles as well as the strong influence of a perpendicularly applied magnetic field on the many-body states. At magnetic fields of the order of 1 T, the cyclotron energy matches the typical energy level spacing, and thus is sufficiently strong to control the behaviour of the quantum dot.

The influence of the electron interactions on the energy spectrum, and in particular, on its magnetic-field dependence was confirmed by exact diagonalization studies performed on simplest systems of three and four electrons [12]. A detailed exact-diagonalization study of the interactions of two-particle system (the quantum-dot helium) was also performed [13] specifically concentrating on peculiarities of the far-infrared response. The point is that in a perfect parabolic confinement the centre-of-mass and the relative motion of electrons decouple, and as a result, the effects of the electron interaction are absent from the far-infrared absorption spectrum. This effect is known as the generalized Kohn theorem [12, 14–16].

The aforementioned exact diagonalization approach [17–19] involves a numerical diagonalization of the fully interacting many-body Hamiltonian in the basis of configurations constructed by distributing electrons over single-particle states in all possible ways. In this context, the word *exact* is used to emphasize that no approximations are used to describe the interparticle interactions. However, in practical work the nominally infinite set of configurations has to be truncated at some point, which naturally introduces a certain error. Problems involving a small number (let's say, $N \leqslant 6$) of particles, or restricted to extreme magnetic fields, can be successfully tackled with this technique since present computational facilities allow to include a sufficient number of configurations in order to obtain convergent results. However, the computational demands grow exponentially with the size of the system, and preclude the use of the exact diagonalizations as a generic method.

Therefore, various single-particle approaches are routinely applied to calculate the properties of few-electron quantum dots. In particular, standard methods of atomic and molecular physics – such as the Hartree, Hartree–Fock, and density functional theory – have been extensively exploited [1, 20–23]. At high electron densities the physics is dominated by quantum degeneracy, and the interparticle interaction acts a rather weak correction. Thus, in this limit the above-mentioned approaches produce accurate and, one might say, unsurprising results. In the opposite – dominated by strong

interactions – limit the spin- and space-unrestricted Hartree–Fock calculations were used to produce broken symmetry states in quantum dots [24]. The obtained ground states showed the incipient Wigner crystallization, that is, the formation of charge density lumps in spite of the fact that the confining potential used in these calculations had a perfect circular symmetry. Broken-symmetry solutions were also obtained from calculations based on the density functional theory [25], which led to some controversy and a debate [23]. In contrast, the ground states obtained from the exact-diagonalization approach always have the symmetry of the Hamiltonian. The internal structure of a quantum dot is somewhat hidden. It can be observed by considering the charge density correlation function, not the charge density itself [17, 26].

Leaving aside the subtleties of computational procedures, let us concentrate on the physical aspect: strong correlation between the particles leads to formation of structures. The ultimate limit of this process is, of course, the celebrated Wigner crystal [27–30] suggested as the ground state of a low-density electronic system back in 1934 [27]. However, even before the Wigner crystal is formed in the extreme limit of strong correlations, its various precursors – such as charge density waves [1] and the angular momentum transitions [17, 26] – are detected.

The physics behind the angular momentum transitions is easy to explain without resorting to detailed calculations. It is not surprising that the electrons confined within a quantum dot in the strong interaction regime tend to stay as far apart as possible. This makes them populate orbitals characterized by high values of the angular momentum. As a result, the total angular momentum of the dot increases in abrupt jumps as the effective coupling strength (set by the external magnetic field) increases. The ensuing charge redistribution in a quantum dot is significant and was successfully measured in an experiment [31].

Let us emphasize that crystallization demonstrates the dominance of the (classical) potential energy over the quantum-mechanical kinetic energy. The ratio of these two characteristic energies is given by the parameter λ. The reciprocal of the same parameter is the measure of the importance of quantum effects. Thus, crystallization and quantum mechanics are mutually exclusive. The quasiclassical regime is the one where interactions and their consequences are important. The quantum mechanical effects are weak, and can be accounted for in a perturbative approach. We were successful to build a coherent theory based on these ideas [32, 33], and the main goal of the present review is to discuss the quasiclassical regime.

In this review, we shall cover in detail the following issues: (i) the enhancement of the relative strength of the electron interactions by the magnetic field, (ii) the Wigner crystallization, (iii) the effect of the quantum mechanics on the structural transitions, (iv) classical power-law behaviour in the energy spectra, (v) global and local currents in a Wigner crystal, and (vi) the role of dissipation in quantum phenomena.

2. Renormalized perturbation series

In the natural atoms the interaction parameter λ is of the order of unity, and the importance of correlations is not overwhelming. Therefore, the atomic theory is successfully developed on the basis of effective single particle approaches. The correlation energy – which, by definition, includes everything that is overlooked by the Hartree–Fock approximation – is a small correction, and can be taken into account in a perturbative approach.

An analogous strategy is clearly unsuitable for parabolic quantum dots. The interaction constant λ is, in general, greater or even much greater than unity. The electron system in a quantum dot is indeed strongly correlated, and a straightforward expansion in powers of λ is not a very promising way to proceed. A direct diagonalization of the many-body problem, on the other hand, is too demanding in terms of computational resources. Thus, development of reliable approximate schemes is of great interest.

We proposed to calculate the energy spectra of strongly correlated quantum dots using the renormalized perturbation series [34, 35]. The basic idea of the series renormalization is to supplement the ordinary few-term energy expansion in powers of λ with the information available from the consideration of the extreme opposite limit ($\lambda \to \infty$). The latter limit is particularly advantageous due to its classical nature. Here, the kinetic energy is comparatively small, and a few-electron system may be represented as a small crystallite performing harmonic vibrations in the vicinity of its lowest-energy configuration.

In both limits of small and large values of the interaction constant λ, we were able to construct two-term expansions. In the limit $\lambda \to 0$ the behaviour of the energy levels is described by the usual first-order perturbation series

$$E(\lambda) = E_0 + E_1\lambda\,. \tag{6}$$

The energy E_0 characterizes a noninteracting system, and is straightforwardly calculated as the sum of single-electron energies. The second expansion coefficient E_1 is obtained by diagonalizing a matrix built from two-particle Coulomb matrix elements.

In the limit of very strong interactions, the two-term expansion becomes

$$E(\lambda) = c_0\lambda^{2/3} + c_1\,. \tag{7}$$

The form of the first term follows directly from the dimensional considerations, which indicate that the radius of the electron system scales as $R \sim \lambda^{1/3}$. The interaction energy is thus proportional to $\lambda^{2/3}$. The second term in the expansion (7) is obtained by considering the vibrations of a ring of $N \leqslant 5$ particles. The vibrational energy levels turn out to be λ-independent.

The interpolation between the two limits is facilitated by introduction of a generalized Hamiltonian

$$H = \frac{1}{2}\sum_{i=1}^{N}(-\xi^2\nabla_i^2 + \boldsymbol{r}_i^2) + \lambda\sum_{i>j}\frac{1}{|\boldsymbol{r}_i - \boldsymbol{r}_j|}\,. \tag{8}$$

Here, the parameter ξ plays the role of the inverse electron mass and the original problem is recovered by setting $\xi = 1$. The generalized Hamiltonian, as well as its eigenvalues, satisfies the scaling relation $H(\xi,\lambda) = \xi H(1,\lambda\xi^{-3/2})$. This relation helps map the strongly interacting regime of the original problem ($\lambda\to\infty, \xi = 1$) onto a generalized problem characterized by finite parameter values, $\lambda = 1$ and $\xi \to 0$. A convergent four-term series is then constructed.

The technique of renormalized perturbation series was first applied to the simplest two-electron quantum dot [34]. The calculated energy values coincided with the results of numerically exact calculation to within 1% for all values of the coupling constant λ. This success motivated us to adapt the technique for larger parabolic quantum dots [35]. Here, the theory has to be expanded to include a somewhat more involved symmetry classification of the energy levels in the two limits. The obtained accuracy is also very satisfactory. We attribute the reasons of success to the softness of the parabolic confinement since the application of the renormalized series to hard-wall quantum dots was not as successful [36, 37]. This demonstrates the importance of analytic properties of the potential for the renormalization procedure. On the other hand, the technique turned to be insensitive to the particle statistics, and we successfully applied the renormalized perturbation series to parabolically confined bosonic systems [38], which are important in the Bose-Einstein condensation studies.

3. Influence of quantization on the phase transition

Seeking to understand a complicated many-body phenomenon, such as crystallization, it is worthwhile to start from the simplest system of just two interacting electrons. Very often consideration of a simplified model problem produces analytical results and gives an approximate qualitative picture reflecting the phenomena that take place in the real many-electron system. Sometimes, one is even able to extract reliable estimates of the parameters that are responsible for the features of the considered many-particle system.

In order to reveal the role of quantization in the electron crystallization as an order-disorder phase transition, we calculated the quantum-mechanical spectrum of a two-electron artificial molecule composed of two vertically coupled two-dimensional single-electron quantum dots [39]. To be fully precise, in quantum dots and other finite systems one should speak not of phase transitions but rather of bifurcations that play the role of phase transitions.

A classical study of the above artificial molecule was carried out in Ref. [40]. The centre-of-mass motion of the two-electron system contributes only an energy shift, which is not important for our purposes. The relative motion is then described by the potential

$$U(r) = \frac{1}{4}m^*\omega_0^2 r^2 + \frac{e^2}{\epsilon}\sqrt{r^2+d^2}\,, \tag{9}$$

dependent on the relative coordinate $\boldsymbol{r} = \boldsymbol{r}_1 - \boldsymbol{r}_2$. Here we use the standard notation whereby m^* is the effective electron mass, ϵ is the dielectric constant of the medium, and ω_0 is the frequency of the radial electron confinement.

In this context, it is convenient to introduce nonstandard dimensionless variables expressing the distances in the units of $(e^2/\epsilon\alpha)^{1/3}$, and energies in the units $\varepsilon_0 = (e^2/\epsilon\alpha^2)^{2/3}$. Here $\alpha = m\omega_0^2/2$, and the symbol d stands for the vertical distance between the two dots. In this way, the potential reduces to

$$U(r) = \frac{1}{2}r^2 + \frac{1}{\sqrt{r^2+d^2}}\,, \tag{10}$$

and after minimization leads to the equilibrium radius for the ground-state configuration: $r_0(d) = \sqrt{1-d^2}$ for $d < 1$ and $r_0(d) = 0$ for $d > 1$. We see that the calculated equilibrium radius plays the role of an order parameter. As long as the separation between the dots is larger than the critical value $d = 1$, the two electrons are located on the axis of the molecule. The bifurcation, which occurs at $d = 1$, breaks the symmetry and moves the electrons into their new equilibrium

positions off the symmetry axis. Inserting the values of the radius $r_0(d)$ into the potential (10) we also calculate the equilibrium energy and (aiming to determine the nature of transition) the derivatives of the energy with respect to the distance d. The results read:

$$E = (3-d^2)/2, E' = -d, \quad E'' = -1, \quad d < 1\,,$$
$$E = 1/d, \quad E' = -1/d^2, E'' = 2/d^3, d > 1\,. \tag{11}$$

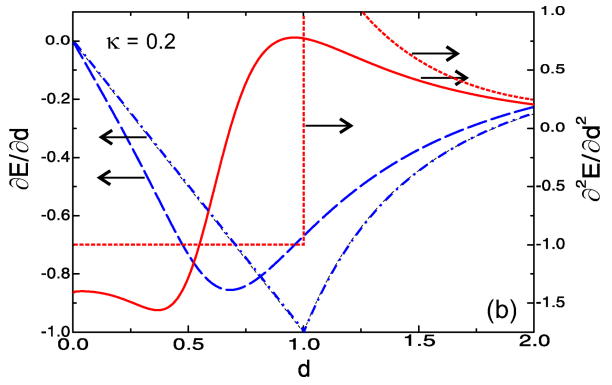

Fig. 1. The first and second energy derivatives as a function of the distance d. The classical result: the first (second) derivative is plotted by the blue online dash-dotted (red online dotted) curve. The quantum-mechanical result: the first (second) derivative is shown by the blue online dashed (red online solid) line.

The behaviour of the energy derivatives (11) is shown in Fig. 1. The (blue online) dash-dotted curve corresponds to the first derivative, and the (red online) dotted curve corresponds to the second derivative. We see that at the point $d = 1$ the first derivative is continuous, but has a kink, while the second derivative is discontinuous. This behaviour resembles the phase transition of the second kind in the Ehrenfest classification.

Proceeding to the quantum-mechanical description, we construct the Hamiltonian and solve the eigenvalue problem. In the dimensionless variables, the Hamiltonian equals the sum of the classical potential (10) and the operator

$$T = -\kappa^2 \nabla^2\,, \tag{12}$$

which represents the kinetic energy of the relative motion. The dimensionless parameter $\kappa = \hbar\omega_0/\varepsilon_0$ is the ratio of the characteristic quantum-mechanical and classical energies at the transition point, and serves as the measure of the importance of quantization. The derivatives of the ground-state energy are plotted next to the classical results on the same Fig. 1. We see that quantization ruins the sharp phase transition. The kink (jump) in the first (second) energy derivative are eliminated. Nevertheless, in the case of relatively small $\kappa \lesssim 0.1$ values, the imprint of phase transition is still distinct.

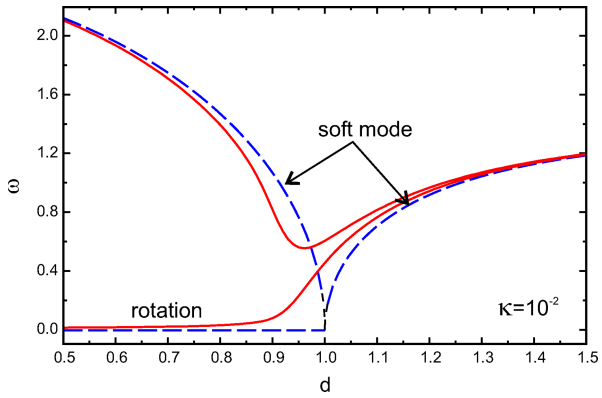

Fig. 2. The quantum-mechanical (solid red online curves) and classical frequencies (dashed blue online curves).

The excitation frequencies are also calculated, and the result is shown in Fig. 2. The classical vibration frequencies are plotted in (blue online) dashed curves and the corresponding quantum mechanical transitions between the excited states are shown by the (red online) solid curves. It is generally known that the presence of a soft mode is an inherent property of the second order phase transition. Indeed, in the classical description of the structural transition in our molecule one of the vibration frequencies goes to zero when the distance d value approaches the critical point. The corresponding quantum-mechanical frequency, however, does not reach the zero value. This is yet another indication that quantization destroys phase transitions.

4. Wigner crystallization

In this section, our goal is to define the criteria that could be used to judge about the formation of internal structure in a quantum dot, and to relate this structure to the involved energy scales and to the interparticle coupling strength. With this in mind, we solve a simplified model discussing the spectrum and the charge density of a two-electron quantum dot [41].

As already mentioned in the previous section, in the case of parabolic confinement the centre-of-mass and the relative motion can be separated. The separation is achieved by introducing the radius-vector of the centre of mass $\boldsymbol{R} = (\boldsymbol{r}_1 + \boldsymbol{r}_2)/2$ and the relative radius vector $\boldsymbol{r} = \boldsymbol{r}_1 - \boldsymbol{r}_2$. As a result, the original problem splits into two independent single-particle problems. In addition, the circular symmetry enables one to write the total wavefunction as a radial part times the angular part

$\exp\{\mathrm{i}(m\varphi + M\Phi)\}$. Here, the uppercase symbols M and Φ denote, respectively, the angular momentum and the rotation angle of the centre-of-mass motion. Likewise, the corresponding lowercase symbols have the same meaning for the internal motion.

The radial wavefunction is, in its own turn, a product of two components describing the centre-of-mass and the relative motion. These components satisfy the respective one-dimensional radial Schrödinger equations with the following dimensionless Hamiltonians:

$$H_R = -\frac{1}{4R}\frac{\mathrm{d}}{\mathrm{d}R}R\frac{\mathrm{d}}{\mathrm{d}R} + \frac{1}{4}\left(\frac{M}{R} - \gamma R\right)^2 + R^2\,, \quad (13a)$$

$$H_r = -\frac{1}{r}\frac{r}{\mathrm{d}r}r\frac{r}{\mathrm{d}r} + \left(\frac{m}{r} - \frac{\gamma r}{4}\right)^2 + \frac{1}{4}r^2 + \frac{\lambda}{r}\,. \quad (13b)$$

Here, all energies are measured in the units $\hbar\omega_0$, and we use the standard definitions for the confinement frequency ω_0, the coupling strength λ, and the dimensionless magnetic field γ.

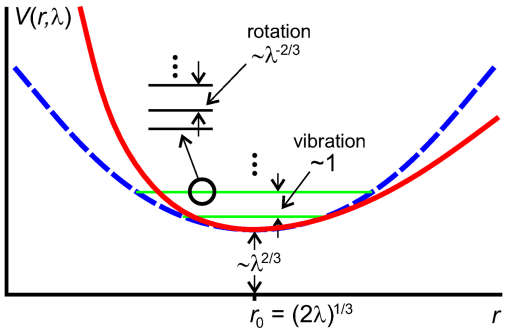

Fig. 3. The potential for the relative motion when $\gamma = 0$ (red online solid curve), the approximate potential (14) (dashed blue online curve), and the vibration and rotation terms indicated by the horizontal lines.

Let us separately consider two variants of the formulated problem: with and without the magnetic field.

It is evident that in the absence of the magnetic field ($\gamma = 0$), the ground state of the centre-of-mass motion corresponds to zero angular momentum ($M = 0$) and gives some constant energy shift which we eliminate by adjusting the origin of the energy axis. Meanwhile, the relative motion can be interpreted as the motion of some fictitious particle in a one-dimensional potential well

$$V(r,\lambda) = \frac{1}{4}r^2 + \frac{\lambda}{r} + \frac{m^2}{r^2}\,, \quad (14)$$

shown in Fig. 3 by the (red online) solid curve.

Restricting the consideration to the interesting limit of strong interactions ($\lambda \to \infty$) the potential (14) can be simplified further. Disregarding the last rotational term in Eq. (14), we find that the potential has its minimum at the point $r_0 = (2\lambda)^{1/3}$. The Taylor expansion of the potential in vicinity of the minimum point reads

$$V(r,\lambda) \approx \frac{3}{4}(2\lambda)^{2/3} + \frac{3}{4}(r - r_0)^2 + \frac{m^2}{(2\lambda)^{2/3}}\,. \quad (15)$$

We see that there are three energy scales involved. The largest one appears in the first term (which is of the order of $\lambda^{2/3}$), and includes the interaction plus the confinement. This classical potential is responsible for the electron structure in the quantum dot. (The minimum of the potential can serve as a means for the Wigner crystal definition.) The second part defines the intermediate energy scale. This potential term, together with the kinetic energy operator in the Hamiltonian (13b), leads to the quantum-mechanical problem of the crystal vibrations. As this contribution does not depend on λ, the separation of the vibrational levels is of the order of unity. This result justifies the proposed scheme of calculation based on the potential expansion in powers of $\lambda^{-2/3}$. It consists of the classical calculation of the electron system structure followed by the quantum-mechanical treatment of its vibrations in the harmonic approximation. The remaining term in Eq. (15) contributes the fine rotational structure to the obtained vibration terms. All these energy scales are shown in Fig. 3 by corresponding horizontal lines.

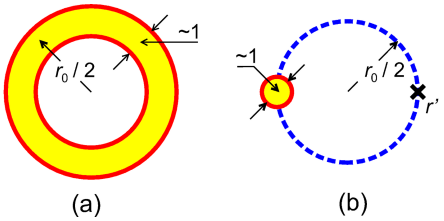

Fig. 4. Schematic view of (a) the electron density and (b) the correlation function (b) in the quasi-classical limit when $\lambda \to \infty$.

In the simple case of two electrons we obtain an explicit expression for the wavefunction in the ground state

$$\Psi(\boldsymbol{r}_1, \boldsymbol{r}_2) \sim \exp(-R^2)\exp\{-a(r - r_0)^2\}\,, \quad (16)$$

where $a = \sqrt{3}/4$. Integrating the squared absolute value of the wavefunction (16) over the coordinates of one electron, we obtain the electron density in the dot, which is shown schematically in Fig. 4(a). Due to the circular symmetry of the dot, the crystal structure is not seen, however, the concentration of the electron density on a ring indicates that such structure might be present. The Wigner crystal can be directly seen in the correlation function that is equal to the squared absolute value

of the same wavefunction (16) considered as a function of the coordinates of one of the electron. The position of the other electron is fixed at a certain point $\boldsymbol{r}'$ chosen, e. g., on the circle of radius $r_0/2$, as shown in Fig. 4(b). We see that in this case the density of the free electron is concentrated around the antipodal point on the same circle.

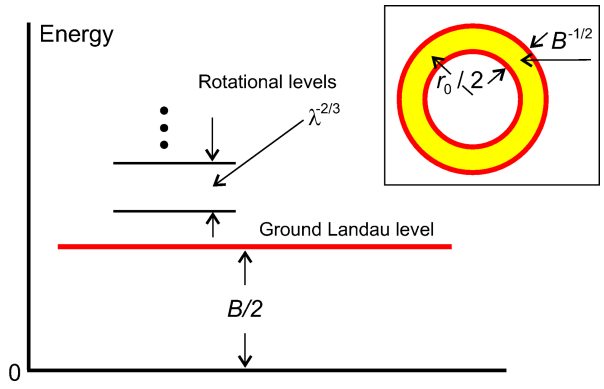

Fig. 5. Energy spectrum in the case of strong magnetic field. The energy is given in $\hbar\omega_c$ units. Electron density in the inset.

In the case with a strong magnetic field, a similar analysis can also be carried out, although it is more laborious. Its main result is summarized in Fig. 5. The approach is based on minimization of two expressions: the term that appears in the parentheses in Eq. (13b), and the sum of the last two terms in the same equation. This procedure leads to the equilibrium radius $r_0 = (2\lambda)^{2/3}$ and the ground-state angular momentum $m_0 = \gamma r_0^2/4$. The expansion of the potential in the vicinity of these values leads to

$$\left(\frac{m}{r} - \frac{\gamma r}{4}\right)^2 \approx \frac{\gamma^2}{4}(r - r_0)^2 + \frac{(m - m_0)^2}{(2\lambda)^{2/3}}. \quad (17)$$

The first (largest) term together with the kinetic energy operator in the Hamiltonian (13b) gives the largest contribution to the energy. Actually it produces the Landau levels. So, in contrast to the situation without the magnetic field, now the main contribution to the energy spectrum is quantum-mechanical. It leads to the following dimensions of the radial wave function $\Delta r \sim B^{-1/2}$. Fortunately, in the limit of a strong magnetic field and low temperature, the electrons are frozen in the lowest Landau level, and the Wigner crystallization follows from the same minimum of the confinement and the interaction potential. Comparing (15) and (17) we see that the Landau levels play the role of the Wigner crystal vibrations and – as we explained above – are frozen. The crystal dynamics contains only the rotational modes whose energies are of the same order of magnitude as in the previous case without the magnetic field.

The electron density is shown in the inset of Fig. 5. It looks like the previous ring of the same radius, but the thickness of this ring is significantly smaller. That is why we may to conclude that the strong magnetic field favours crystallization.

5. Angular momentum transitions

Formation of structures and structural transitions in quantum dots – as well as in any other many-particle system – are among the most complex and demanding physical problems. The key factor involved in these phenomena is the strong interaction between the particles which makes the problem inseparable. We were fortunate to formulate several simple models, treated in Sections 3 and 4, that are solvable analytically and demonstrate structural transitions in few-electron quantum dots. When confronted with more complicated models, however, we had to resort to numerical approaches which define the subject of the present section.

As already mentioned in the Introduction, a rather special role is played by the method of exact diagonalizations [17–19]. In this approach, one first solves the simple problem of a single electron moving in a quantum dot, and obtains a complete set of single-particle eigenfunctions and the corresponding energies. The starting basis for problems involving N electrons is then constructed in a combinatorial fashion, i. e., by distributing the electrons over the available orbitals in all legitimate ways. This task is greatly simplified by the presence of a circular symmetry, as many particle states of different total angular momenta L are not coupled by the Hamiltonian and can be treated separately.

In this manner, the Hamiltonian operator is represented as a set of matrices – one for each angular momentum of interest – which can be diagonalized numerically. The matrix is, in principle, infinite dimensional and has to be truncated by restricting the basis of many-particle states according to some criteria. In our work, we typically choose to include all many-body states for which the sum of N single-particle energies does not exceed a given threshold energy. The accuracy of the results depends essentially on our ability to use a sufficiently large threshold. To give a specific example, in calculations performed on four-electron quantum dots, we needed (sparse) matrices of around $20\,000$ rows and columns, and were able to obtain energies accurate to

four significant digits [17]. We extended our calculations to quantum dots containing five and six particles [26]. The computational effort grows exponentially with the system size, and calculations for even larger systems turned out to be beyond reach.

We should note that due to its ability to provide accurate results, the exact-diagonalization approach proved to be very useful as a reference against which the reliability and accuracy of various approximation schemes could be tested and gauged. In particular, this method played the role of a benchmark numerical experiment when developing the multicentre-basis Hartree–Fock approach [20] as well as the quasiclassical theory further discussed in Section 8.

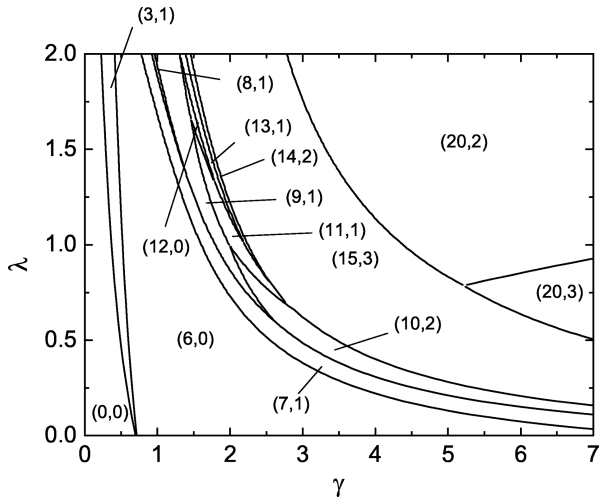

Fig. 6. Ground-state angular momentum transitions in a six-electron quantum dot.

Figure 6 shows a typical result obtained by means of an exact-diagonalization study: the ground-state phase diagram of a six-electron parabolic quantum dot placed into a perpendicular magnetic field. Phase diagrams of this type were obtained also for quantum dots containing a smaller number of electrons [17, 26]. They succinctly summarize the transformation of the ground state as a function of the effective coupling strength λ and the dimensionless magnetic field strength γ.

The solid lines in Fig. 6 signify the phase boundaries. They partition the two-parameter phase space into areas corresponding to the different ground states of the quantum dot. The ground states are labeled by the pairs of numbers in parentheses (L, S). The quantum number L is the total angular momentum of the state and $S = 0, 1, 2, 3$ is the total spin. While the interaction strength λ is difficult to modify, the magnetic field γ can be easily varied in a broad range of values. We see that with increasing magnetic field, states of ever higher angular momenta are competing to become the ground state. This results in a sequence of angular momentum (and spin) transitions and an ensuing redistribution of electron charge in a quantum dot [31].

The ground-state phase diagram in Fig. 6 shows that, in general, a large number of ground states are realized at different values of the coupling strength and the magnetic field. However, one notes that some of ground states are significantly more stable than the others: they control relatively large portions of the phase space. The most conspicuous are the so-called *maximum density droplet* (MDD) states characterized by a peculiar distribution of electrons over the single-particle orbitals [17, 21]. In these states, correlation arranges electrons in such a way that their single-particle angular momenta form an arithmetic progression with difference equal to unity.

The first MDD state is the spin-unpolarized state $(6, 0)$ seen in Fig. 6. Here, the electrons occupy orbitals with the angular momenta $l = 0$, 1, and 2. Each orbital accommodates two electrons of opposite spin. It is not difficult to see that the single-particle angular momenta add to six, and the total spin is zero. The second MDD state is the spin-polarized state $(15, 3)$. Here, the magnetic field is sufficiently strong to force all spins to be aligned, and the electrons occupy six consecutive orbitals with the single-particle angular momenta $l = 0$, 1, 2, 3, 4, and 5 so that the total angular momentum adds up to $L = 15$.

The exact-diagonalization method also provides the complete information about the many-particle wavefunction. This wavefunction depends on the coordinates of all electrons and is hard to analyse. Therefore, reduced quantities must be constructed. An obvious first choice is the single-particle charge density. However, the charge density fails to fully demonstrate the crystallization of electrons in a quantum dot as this quantity retains the circular symmetry of the Hamiltonian. As a result, the charge density reveals only the formation of the ring structure and not the azimuthal correlations.

In order to fully uncover the internal structure of a few-electron system trapped by a circular confinement, one has to go one step further and consider the density-density correlation function. The physical meaning of the correlation function can be (somewhat loosely) interpreted as the *conditional density*. It shows the conditional probability to find an electron at a given point $\boldsymbol{r}$ provided that another electron is pinned at a fixed position $\boldsymbol{r}'$. This result can be plotted on a two-dimensional graph and visualizes the formation of a Wigner crystal.

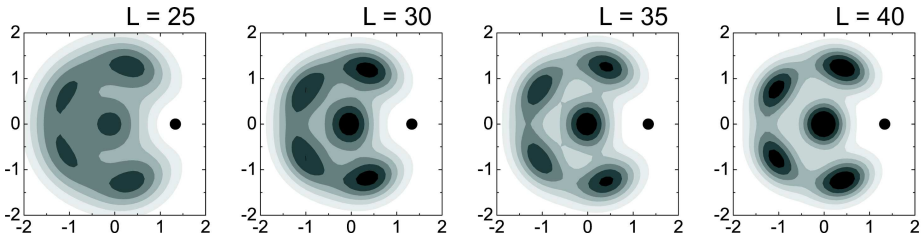

Fig. 7. Wigner crystallization in a six-electron quantum dot.

An illustrative example is given in Fig. 7. Here we show how the crystal structure in a six-electron quantum dot gradually sets in as the magnetic field is increased. The four panels of Fig. 7 are labeled by the values of the ground-state angular momentum which changes from $L = 25$ to 40. One of the electrons is pinned in the position marked by the black dot at the intersection of the maximum-density ring and the x axis. The remaining five electrons tend to localize close to their classical lowest-energy positions, and the localization conspicuously improves with increasing magnetic field.

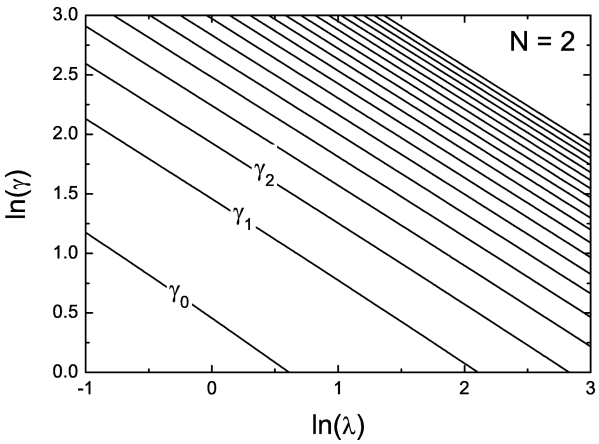

Fig. 8. Critical magnetic fields plotted as a function of the coupling strength in a two-electron quantum dot.

6. Power law

In this section we will draw closer attention to the quantitative characteristics of the structural transitions in strongly correlated quantum dots. As we learned in the preceding section, the ground-state angular momentum transitions play the role of a distinctive phenomenon which reflects the formation of structures inside a quantum dot. In a nutshell, these transitions occur when the external magnetic field strength reaches certain characteristic values, and the angular momentum quantum number in the ground state suddenly jumps to a higher value.

We performed a numerical investigation in order to determine how the critical values of the magnetic field depend on the interaction strength λ. It turns out that the obtained dependences closely follow a power law [42]

$$\gamma_L = a_L \lambda^b \,. \tag{18}$$

Here, γ_L is the critical value of the dimensionless magnetic field. As the magnetic field crosses this value, the ground state of a quantum dot switches from the one characterized by the angular momentum L to the following in order, typically with the angular momentum $L+1$. The quantity a_L is the proportionality factor dependent on both the angular momentum L and the number of electrons in the dot. Figure 8 presents the most clear-cut illustration of the mentioned power-law behaviour of the critical magnetic fields. This figure pertains to the simplest two-electron quantum dot. Similar figures have been obtained for three- and four-electron quantum dots as well [42].

The dependence (18) is very simple indeed; its validity made us realize that the considered phenomenon of structure formation must be essentially classical. Incidentally, let us mention that power laws also describe the internal structure of the many-particle correlation functions [43].

Naturally, having obtained such a simple relation (18) from a numerical calculation, we felt obliged to seek a more thorough understanding. Thus we attempted, and succeeded, to derive the power law analytically [42].

The analytical treatment starts from the basic fact that in the limit of strong interactions (in fact, strong magnetic fields) a parabolic quantum dot containing not more than five electrons is transformed to a polygonal electron ring. That is, all N electrons are arranged equidistantly on a ring surrounding the centre of the confinement. As the first step of our analytical solution we are able to exclude the magnetic field. Thus the energies of the original problem $E(\lambda, \gamma, L)$ can be expressed in terms of solutions of the modified model

$E_0(\lambda_0, L)$ with no magnetic field but with a scaled value of the coupling constant

$$\lambda_0 = \lambda \left[1 + \frac{1}{4}\gamma^2\right]^{-1/4} . \tag{19}$$

The relation between the two energies reads

$$E(\lambda, \gamma, L) = E_0(\lambda_0, L) \left[1 + \frac{1}{4}\gamma^2\right]^{1/2} - \frac{1}{2}\gamma L , \tag{20}$$

and the dimensionless state energies obtained from the zero-field model are

$$E_0(\lambda_0, L) = L + \lambda_0 \sqrt{\frac{N}{L}} f_N . \tag{21}$$

Here f_N is a geometric structure factor whose values are $f_2 = \frac{1}{2}$, $f_3 = \sqrt{3}$, and $f_4 = 1 + 2\sqrt{2}$. The critical γ values can now be easily found from the defining equation $E(\lambda, \gamma_L, L) = E(\lambda, \gamma_L, L + 1)$. The results show that the critical magnetic fields indeed obey the power law

$$\gamma_L = \frac{2}{(N f_N^2)^{1/3}} \left(L + \frac{1}{2}\right) \lambda^{-2/3} . \tag{22}$$

We would like to make two interesting observations. First, note that the power law exponent has a universal value $b = -\frac{2}{3}$ which is the same for any number of electrons in the quantum dot and any state. Second, it is generally not so surprising that the obtained power law is valid in the classical limit of large values of the angular momentum quantum numbers L. However, it turns out to be working perfectly also in the quantum-mechanical regime for the angular momenta $L \leqslant 10$.

This result convinced us that the classical approaches are very robust even in the traditionally quantum-mechanical realm where discreetness of quantum numbers is significant. Therefore, it is worthwhile to further develop approximate calculation schemes based on classical notions and valid in more general situations that were considered now. The main virtue of the classical (or more precisely, quasiclassical) approaches lies in their relative simplicity and ability to provide results that are accurate and easy to comprehend without resorting to heavy computations.

7. Local currents

Further development of the quasiclassical theory of quantum dots leads naturally to the question of currents that are induced in a quantum dot when a strong perpendicular magnetic field is applied. This problem arises from the representation of the Wigner crystal as a rotating electron molecule [44]. One of the main issues here is the near compensation between a strong magnetic field on the one hand, and the high angular momentum value of the ground state on the other hand. The magnetic field strength can have an arbitrary value whereas the angular momentum is necessarily quantized. This conflict leads to the appearance of the so-called *persistent currents* [45] recently observed in experiments on nanoscopic ring-shaped conductors [46]. Persistent currents are dissipationless electric currents induced by a static magnetic field. They do not require an external power source, however, the survival of the electron phase coherence along the path is crucial. These issues led us to consider the rotation of a few-electron quantum dot – to be more precise, a single electron ring – in a strong magnetic field [33, 47, 48].

When dealing with the rotation of the system as a whole, it is helpful to switch to the rotating frame of reference. The straightforward formulation of the Hamiltonian of the problem is, however, not easy since the definitions of the canonical coordinates and momenta in a rotating frame may be tricky. Thus, following the suggestion of earlier authors [49] we: (i) start with the Lagrangian, (ii) perform the change of coordinates in order to switch to the rotating frame, (iii) define the canonical variables, and (iv) arrive at the Hamiltonian using the standard procedure.

The system of N two-dimensional electrons possesses $2N$ degrees of freedom. One of the modes is special – it corresponds, as expected, to the rotation of the system as a whole. The remaining $2N - 1$ modes correspond to various vibrations. We were able to present the total ground-state wavefunction in a remarkably simple form [47]

$$\Psi = \mathrm{e}^{\mathrm{i}M\chi} \mathrm{e}^{-\gamma K/4} . \tag{23}$$

The first exponent describes the rotation with χ being the collective rotation angle. The second factor is a multidimensional Gaussian which represents the vibrational ground state. Here,

$$K = \sum_{i=1}^{N} \left(x_n^2 + y_n^2\right) + \frac{1}{N}\left(\sum_{i=1}^{N} x_n\right)^2 - \frac{1}{N}\left(\sum_{i=1}^{N} y_n\right)^2 , \tag{24}$$

and x_n (y_n) represent the local deviations of the nth electron from the equidistant positions on a ring in the angular (radial) directions.

The knowledge of the complete ground-state wavefunction enables us to calculate the charge and current distribution in the quantum dot which are shown in Fig. 9. Due to the circular symmetry of the confinement

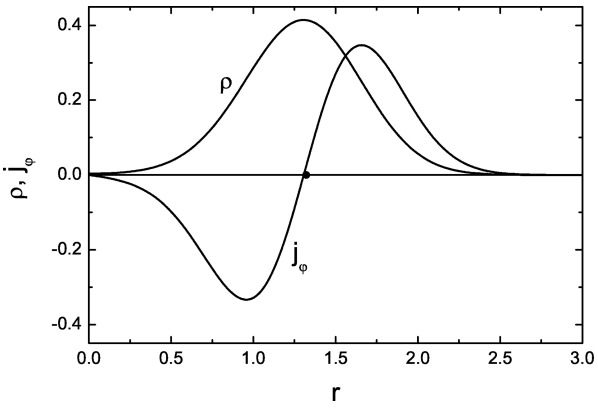

Fig. 9. Distribution of the charge and current density in a quantum dot.

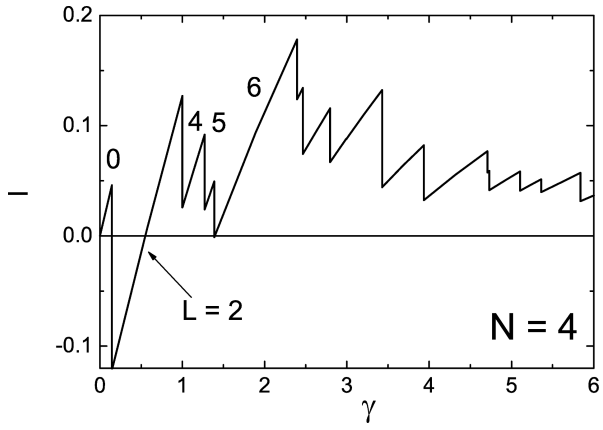

Fig. 10. Persistent currents in a four-electron quantum dot.

these distributions are also circularly symmetric, and the current density has only the azimuthal component j_φ. Thus it suffices to plot only the radial dependences of the charge density ρ and j_φ. Figure 9 corresponds to a three-electron quantum dot with the coupling constant set to $\lambda = 4$, and the dimensionless magnetic field is such ($\gamma = 6.8$) that the ground state has the angular momentum $L = 18$. The radial dependence of the current density is nearly antisymmetric with respect to the classical dot radius. Thus the current has two components flowing in the opposite directions in the interior and the exterior of the electron ring. The two components nearly cancel each other, however, the cancellation is not complete, and there is a finite net azimuthal current given by

$$I = \int_0^\infty \mathrm{d}r\, j_\varphi(r)\,. \tag{25}$$

The current (25) is precisely the quantum-dot version of the persistent currents in metal rings. The magnetic field dependence of the persistent current is plotted in Fig. 10. The shown dependence clearly displays a sawtooth-like behaviour, and the sudden drops of the net current correspond to the abrupt changes of the ground state. The angular momenta of the involved ground states are indicated by numbers.

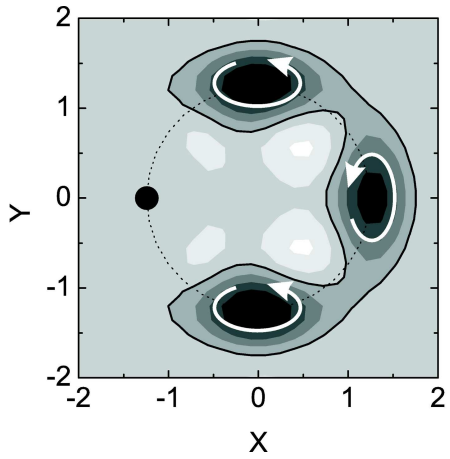

Fig. 11. Vorticity of the local current in a four-electron quantum dot.

The persistent currents reflect the global rotation of the electron system in a quantum dot. Besides this global motion, the local currents corresponding to the Larmor circulation of individual electrons in the vicinity of their classical positions can also be calculated. Due to the anisotropy of the local confinement felt by an electron these currents are not circular but rather elliptic – elongated in the azimuthal direction. Figure 11 shows the vorticity of the local currents (the curl of the current density field). In order to rid of the global rotation and be able to concentrate on the local circulation we pin one of the electrons at the position marked by the black dot on the classical ring. The remaining three electrons are localized close to their classical positions. Dark (light) areas correspond to the areas of positive (negative) current vorticity. These areas are delimited by the line of zero vorticity marked by a solid black line. It is interesting to note that local currents were also observed in density-functional calculations that produce broken internal symmetry states [25]. In this approach the currents are available directly from the Kohn-Sham orbitals and one does not need to consider correlation functions.

8. Quasiclassical theory

Our early work devoted to the quasiclassical treatment of quantum dots was restricted to the simplest case – when the lowest energy configuration is a single polygonal ring accommodating all electrons. This simple picture is valid only as long as the number of

electrons in a parabolic confinement does not exceed five. When the number of electrons is six or more, one typically observes a system of concentric rings. Thus, for example, the ground state of a 19-electron quantum dot features a single electron located at the centre of the quantum dot which is surrounded by an inner ring of six electrons plus an outer ring of twelve electrons. In order to be applicable to quantum dots with an arbitrary number of electrons, the quasiclassical approach of the previous sections has to be generalized.

The essential idea of the quasiclassical theory [32, 33] is to employ a perturbative approach based on the expansion in the inverse powers of the dimensionless magnetic field. As mentioned before, the physics of quantum dots is determined by the strength of the interparticle interactions which are set by the magnetic field. These observations suggest the choice of the magnetic field strength as the control parameter.

The zeroth-order term in the expansion corresponds to the limit of an infinitely strong magnetic field. In this limit, the electron spectrum is transformed into a ladder of Landau levels separated by very large (proportional to the magnetic field) gaps. The electrons become confined to the lowest Landau level and their motion is thus frozen out. The absence of dynamics enables us to significantly simplify the problem at hand by disregarding the kinetic energy term. Note that this in turn implies disregarding the quantum mechanics, as the Planck's constant is present only in the kinetic energy term. Therefore, in this limit we are left with a purely classical problem.

The task of the classical limit is the determination of the stable configurations defined as the minima of the total potential energy of N interacting particles in a parabolic confinement

$$V = \frac{1}{2}\sum_{i=1}^{N} r_i^2 + \sum_{i=1}^{N}\sum_{j>i}^{N} \frac{1}{|\boldsymbol{r}_i - \boldsymbol{r}_j|}\,. \qquad (26)$$

Note that since the kinetic energy is absent from the problem, we define the scaled variables by balancing the confinement and coupling terms. Thus, the coupling constant λ is included in the definition of the length unit $r_0 = (\lambda/m^*\omega^2)^{1/3}$, which is used in this section, and does not appear in the potential (26).

The problem posed by Eq. (26) is not a trivial one. The energy to be minimized is a complicated function of $2N$ arguments, and typically, besides the global energy minimum, one finds a number of local energy minima – the so-called metastable configurations. The number of metastable configurations is known to grow as the exponent of the number of particles, and reaches hundreds already for systems containing just a few dozen particles [50].

The minimization of the potential energy in the multidimensional configuration space can be successfully tackled by means of: (i) direct minimization techniques, such as the steepest descent, conjugate gradient or the Newton optimization [51], (ii) various thermodynamic approaches, most importantly the Simulated annealing algorithm and Molecular dynamics [51, 52], and (iii) evolutionary approaches such as the genetic algorithm [53]. The first systematic study of the ground-state configurations of classical artificial atoms was presented in Ref. [54]. Using the simulated annealing and direct minimizations, we are able to reliably determine the ground state as well as all metastable states of systems containing up to 40 particles. Some of the ground-state configurations are depicted in Fig. 12.

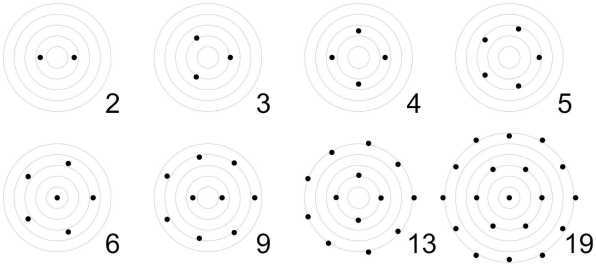

Fig. 12. Some ground-state configurations of classical systems in a parabolic confinement.

In a strong (but not infinitely strong) magnetic field one has to pay attention to the dynamics of electrons in the quantum dot. The dynamics primarily involves small collective oscillations in the vicinity of the ground state configuration. However, due to the circular symmetry of the Hamiltonian there is, in addition, a rotational mode. In spite of its relation to the symmetry, in practical matters this mode is a complication, and one has to switch to the rotating frame of reference in order to decouple the rotational and vibrational motion [32, 47–49].

Moreover, it turns out that rotation is not the only special mode. One of the vibrational modes is also rather peculiar, and is known as the breathing mode [55]. In this mode, all electrons perform strictly radial oscillations to and from the centre, and the amplitude deviations and velocities of all the electrons are proportional to their respective radial distances from the centre of the quantum dot. In this sense, the breathing mode is indeed very similar to the rotational mode. Note that when the quantum dot rotates as a whole, the velocities of individual electrons are also proportional

to their radial coordinates, however, their directions point perpendicularly to their radius-vectors.

Having successfully singled out the two special modes we are left with an ordinary vibrational problem in a magnetic field. The vibrational Hamiltonian can be presented in a particularly elegant manner [32]. To this end we collect all the generalized electron coordinates in a column vector

$$w = (w_1, w_2, \ldots, w_{2N-2})^T , \qquad (27)$$

with the superscript T denoting the transpose. The total number of degrees of freedom is $(2N-2)$ as two modes have been separated, and thus the coordinates w_i are orthogonal to the breathing and rotational modes. The first $N-1$ of these are linear combinations of the radial displacements of the individual electrons, while the remaining half are formed by identical combinations of the angular displacements. The canonical momenta are introduced in a similar fashion

$$W = (\partial/\partial w_1, \partial/\partial w_2, \ldots, \partial/\partial w_{2N-2})^T . \qquad (28)$$

The vibrational Hamiltonian is then cast into the form of a multidimensional harmonic oscillator:

$$H_{\rm vib} = \frac{1}{2}\left(W - \frac{\mathrm{i}\gamma}{2}\mathcal{G}w\right)^2 + \frac{1}{2}w^T V^{(2)} w . \qquad (29)$$

The last term of (29) is a quadratic form written in a matrix notation, which represents the second order expansion of the potential around its minimum point, and the symbol $\mathcal{G}$ represents an auxiliary rotation matrix.

The ground state of (29) is a Gaussian function in $2N-2$ dimensions

$$\Psi_{\rm vib} = \exp\left(-\frac{\gamma}{4}w^T \mathcal{X} w\right) , \qquad (30)$$

where the matrix of coefficients $\mathcal{X}$ must be obtained by solving the quadratic matrix equation

$$\mathcal{X}^2 + \mathcal{G}\mathcal{X} - \mathcal{X}\mathcal{G} = \mathcal{I} + \frac{4}{\gamma^2}V^{(2)} , \qquad (31)$$

known as the matrix Riccati equation. We solve the quadratic matrix equation by mapping it onto the ordinary spectral problem of an extended $(4N-4)\times(4N-4)$ matrix [47]. The vibrational energy is proportional to the trace of the matrix $\mathcal{X}$

$$E = \frac{\gamma}{4}\mathrm{Tr}\,\mathcal{X} . \qquad (32)$$

The knowledge of the many-body wavefunction paves the way for the investigation of the internal structure of the correlated system of electrons. As explained before, this structure is not directly manifest in the distribution of the (charge) density – which retains the circular symmetry of the Hamiltonian – and thus only the density-density correlation function is suitable for that matter.

Besides clearly demonstrating the crystal formation, our calculation leads to a classification of the emerging structures. Thus when the structural stability is considered, quantum dots may be categorized as either *solid* of *liquid-like*. A structure is liquid-like when easily excitable low-frequency modes are present.

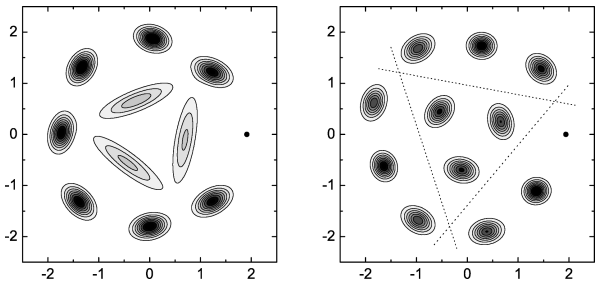

Fig. 13. Solid and liquid-like quantum dots.

Often the presence of a low-frequency mode is connected to the commensurability of the numbers of electrons belonging to neighbouring shells [33]. An excellent illustration of this phenomenon is given by comparison of eleven- and twelve-electron quantum dots in Fig. 13. The system of eleven electrons in a parabolic trap serves as an example of a liquid-like structure. The lowest-energy configuration of the eleven-electron quantum dot consists of two rings: the inner one holds three electrons, and the outer one holds eight. The numbers 3 and 8 are incommensurate, that is, they have no common divisors. As a consequence, the two electronic shells have a nearly circular shape, and the inter-shell rotation is easily excitable thus introducing a low-frequency mode. In Fig. 13 the smooth rotation of the two rings is reflected by the elongated ellipses of the inner shell.

In contrast, the twelve-electron quantum dot is solid and has a rigid structure. The ground-state configuration is again composed of two rings, containing three and nine particles, respectively. This distribution of electrons leads to the emergence of a triangular distortion of the shells, and as a consequence, the inter-shell rotation costs too much energy.

Low-frequency modes of a different nature are also possible [56]. In general, they relate to the presence of two competing minima, that is, minima of comparable depth connected by a transition trajectory that runs

through a saddle point of a rather low energy. Typical examples are: (i) the migration of an electron from one ring into another and (ii) the inter-shell electron exchange.

9. Dissipation in Schrödinger equation formalism

Dissipation is inherently present in any physical system, and dissipative processes play an important role in most experimental measurements since the influx of the probing energy into a system must be counterbalanced by its eventual loss. In many circumstances, one may disregard the details of energy removal processes or account for them in some simple way. However, this is usually not the case when one has to deal with ultrafast processes on the nanometric scale [57].

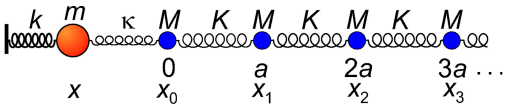

Fig. 14. The layout of the model system.

Traditionally, open quantum systems are treated in terms of the density-matrix formalism [58]. However, the density-matrix formalism has a double set of variables which results in increased computational complexity. We proposed [59–61] to embrace dissipation in a formalism based on the Schrödinger equation, and presented the simplest illustrations, namely, the decay of an excited state of a 1D harmonic oscillator and the nonlinear power absorption.

The considered compound system – consisting of a small quantum system plus a classical heat bath – is shown in Fig. 14. The quantum system is modelled as a harmonic oscillator of mass m and spring constant k, depicted by the large red ball and described in terms of the quantum-mechanical position and momentum operators, $\hat{x}$ and $\hat{p}$. The role of the heat bath is assigned to a semi-infinite chain of identical balls (shown as small blue circles) of mass M interconnected by springs of equilibrium length a and spring constant K. The two subsystems are linked by a weak spring (spring constant κ) connecting the quantum oscillator to the leftmost – the 'zeroth' – ball of the classical chain. The corresponding Hamiltonian reads

$$H = \frac{1}{2m}\hat{p}^2 + \frac{k}{2}\hat{x}^2 + \frac{\kappa}{2}(\hat{x}-x_0)^2 + \sum_{n=0}^{\infty}\left[\frac{1}{2M}p_n^2 + \frac{K}{2}(x_n - x_{n+1})^2\right], \tag{33}$$

with x_n denoting the coordinate of the nth ball measured with respect to its equilibrium position, and p_n – the corresponding momentum.

We assume that the quantum oscillator is described by its own wavefunction $\Psi(x,t)$ that solves the Schrödinger equation

$$\mathrm{i}\hbar\frac{\partial}{\partial t}\Psi(x,t) = H\Psi(x,t)\,, \tag{34}$$

with the above Hamiltonian (33), while the dynamical variables of the balls in the chain obey the classical Newton equations

$$\dot{x}_n = \frac{\partial}{\partial p_n}\langle H\rangle, \quad \dot{p}_n = -\frac{\partial}{\partial x_n}\langle H\rangle\,, \tag{35}$$

with the Hamiltonian operator replaced by its quantum-mechanical average over the state of the quantum oscillator

$$\langle H\rangle = \int_{-\infty}^{\infty}\mathrm{d}x\Psi^*(x,t)H\Psi(x,t)\,. \tag{36}$$

In this way, quantum variables and operators do not enter the equations for the classical degrees of freedom, and one obtains a consistent description. This averaging constitutes the main assumption of the quasiclassical approximation, and was used earlier to treat the coupling of classical and quantum degrees of freedom [62].

The linear equations of the chain motion can be easily solved, and the coordinates x_n of all balls are thus expressed in terms of the zeroth ball coordinate x_0. This enables us to obtain the set of dimensionless equations

$$\mathrm{i}\frac{\partial}{\partial t}\Psi(x,t) = H\Psi \equiv \left[\frac{1}{2}\left(\hat{p}^2+\hat{x}^2\right) - \lambda\hat{x}x_0\right]\Psi\,, \tag{37a}$$

$$\frac{\mathrm{d}}{\mathrm{d}t}x_0 + \lambda(l_0/l)x_0 = \lambda\langle x\rangle\,, \tag{37b}$$

where the classical coordinate is measured in units l_0 ($l_0^2 = \hbar/M\Omega$, $\Omega^2 = K/M$) and the quantum coordinate in units l ($l^2 = \hbar/m\omega$, $\omega^2 = k/m$). The coupling constant $\lambda = (\kappa/k)\sqrt{\omega_0 m/\Omega M}$ is small in the adiabatic case ($m \ll M$), which justifies the proposed quasiclassical approach.

When considering the problem of the nonlinear resonance, we extend the Hamiltonian by adding a periodic external force and a nonlinear term:

$$\Delta H = -2\sqrt{2}\hat{x}F\cos(\omega t) + \alpha\hat{x}^4\,. \tag{38}$$

The oscillator wavefunction is expanded into the series of the harmonic oscillator eigenfunctions

$$\Psi(x,t) = \sum_{n=0}^{\infty} a_n(t)\psi_n(x)\,, \tag{39}$$

where $E_n = n + 1/2$, and the functions ψ_n can be expressed in the standard way in terms of the Hermite polynomials. Inserting (39) into Eq. (37) and assuming slow variation in time of the coefficients a_n (the rotating wave approximation), we arrive at the set of equations

$$\mathrm{i}\dot{a}_n = -\left\{\eta E_n - \alpha\langle n|x^2|n\rangle\right\} a_n$$
$$-\sqrt{n}(F+\mathrm{i}\gamma a^*)a_{n-1} - \sqrt{n+1}(F-\mathrm{i}\gamma a)a_{n+1}\,, \quad (40a)$$
$$a = \sum_{n=0}^{\infty} a_n a_{n+1}^* \sqrt{n+1}, \quad \gamma = \lambda^2/2\,, \quad (40b)$$

where $\eta = \omega - 1$ is the detuning.

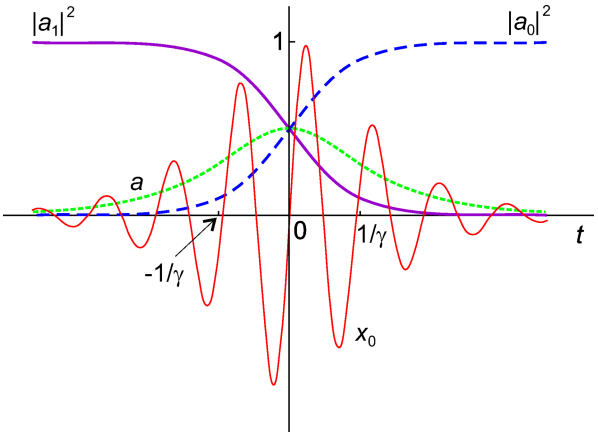

Fig. 15. Decay of a quasistationary state: the probability of the excited state $|a_1|^2$ is shown by the thick solid curve, the probability of the ground state $|a_0|^2$ by the dashed curve, polarization $a = a_0 a_1^*$ by the dotted curve, and the classical chain excitation x_0 by the thin solid curve.

The proposed method is illustrated by considering the decay of a quasistationary state in the two-level approximation. The result is presented in Fig. 15. We note the characteristic time scale of the order of $1/\gamma$ during which the system relaxes from the excited to the ground state. It is remarkable that during this transition an excitation pulse is generated in the classical chain. The pulse carries energy towards infinity which can be regarded as dissipation (energy loss) from the point of view of the quantum subsystem. The energy of this pulse coincides with the difference of the energy levels $E_1 - E_0$ which enables us to conclude that the quantum subsystem causes some quantization in the classical one.

The second example is the resonant nonlinear power absorption which we calculate in the three-level approximation. The typical resonance curves for various degrees of nonlinearity are shown in Fig. 16. We see that in the linear-oscillator case ($\alpha = 0$) the absorption demonstrates the expected Lorentzian behaviour. When nonlinearity increases, the resonant peak moves to the right and becomes asymmetric. Saturation manifests itself as a widening absorption gap close to the shifted resonance frequency. This is in contrast to the classical nonlinear resonance where the power absorption peak is tilted and a hysteresis takes place. The kinks of the resonance curve in the absorption gap are related to various synchronization types between the driving force and the system response. This type of behaviour of the quantum system behaviour is due to the infinite number of degrees of freedom, and reminds the scenarios of appearance of the dynamical chaos in classical systems.

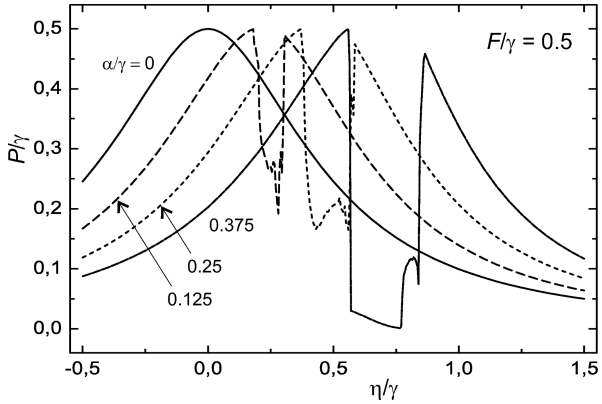

Fig. 16. Power absorption in the three level approximation.

We shall end the presentation of the quasiclassical methods briefly mentioning one more approach – the hydrodynamic method that was applied by Zaremba and co-workers [63] to the quantum dots with a large number of electrons. We applied the hydrodynamic method to the investigation of magnetoplasma excitations in two vertically aligned quantum dots [64]. Two nontrivial results were found in the case when the parabolic confinement of the two dots is not the same. First, the violation of the Kohn's theorem leads to the appearance of modes other than the centre-of-mass ones in the power absorption. Also, the so-called edge modes with small but nonzero oscillator strengths are excited.

The hydrodynamic approach was extended to vertically coupled electron and hole quantum dots [65]. The most conspicuous feature observed in the far-infrared absorption spectra is the anticrossing of two centre-of-mass modes which takes places when the external magnetic field aligns their frequencies. A number of weak edge modes are also present.

10. Conclusions

The following conclusions can be drawn from the discussed issues:

1. In large quantum dots the coupling between electrons is the most important term, and accordingly, the kinetic energy and quantum mechanics play a secondary role.
2. The strong perpendicular magnetic field freezes out the kinetic energy of the electrons, which also contributes to the enhancement of the relative importance of the interparticle interactions.
3. Strongly interacting electron systems in quantum dots and quantum-dot molecules demonstrate formation of structures and structural transitions. Quantum-mechanical effects tend to smear out the otherwise sharp features of these transitions.
4. There exists a well defined quasiclassical regime. In this regime, a rather simple but still potent description based on the classical concepts can be developed. The quantum-mechanical features are successfully included in an perturbative manner.
5. Quantum-mechanical systems are described by fields – the solutions of the Schrödinger equation. In this sense, quantum-mechanical systems have more freedom, and consequently, their behaviour is less stable (more chaotic) than that of their classical counterparts.

References

[1] S.M. Reimann and M. Manninen, Electronic structure of quantum dots, Rev. Mod. Phys. **74**, 1283 (2002).
[2] L.P. Kouwenhoven, D.G. Austing, and S. Tarucha, Few-electron quantum dots, Rep. Prog. Phys. **64**, 701 (2001).
[3] D. Bimberg and N.N. Ledentsov, Quantum dots: lasers and amplifiers, J. Phys. Condens. Matter **15**, R1063 (2003).
[4] V.A. Shchukin and D. Bimberg, Spontaneous ordering of nanostructures on crystal surfaces, Rev. Mod. Phys. **71**, 1125 (1999).
[5] D. Bimberg, M. Grundmann, and N.N. Ledentsov, *Quantum Dot Heterostructures* (Wiley, Chichester, 1998).
[6] Q. Xie, A. Madhukar, P. Chen, and N.P. Kobayashi, Vertically self-organized InAs quantum box islands on GaAs(100), Phys. Rev. Lett. **75**, 2542 (1995).
[7] R.C. Ashoori, H.L. Stormer, J.S. Weiner, L.N. Pfeiffer, K.W. Baldwin, and K.W. West, N-electron ground state energies of a quantum dot in magnetic field, Phys. Rev. Lett. **71**, 613 (1993).
[8] S. Tarucha, D.G. Austing, T. Honda, R.J. van der Hage, and L.P. Kouwenhoven, Shell filling and spin effects in a few electron quantum dot, Phys. Rev. Lett. **77**, 3613 (1996).
[9] M.A. Reed, J.N. Randall, R.J. Aggarwal, R.J. Matyi, T.M. Moore, and A.E. Wetsel, Observation of discrete electronic states in a zero-dimensional semiconductor nanostructure, Phys. Rev. Lett. **60**, 535 (1988).
[10] T.P. Smith, III, K.Y. Lee, C.M. Knoedler, J.M. Hong, and D.P. Kern, Electronic spectroscopy of zero-dimensional systems, Phys. Rev. B **38**, 2172 (1988).
[11] Ch. Sikorski and U. Merkt, Spectroscopy of electronic states in InSb quantum dots, Phys. Rev. Lett. **62**, 2164 (1989).
[12] P.A. Maksym and T. Chakraborty, Quantum dots in a magnetic field: Role of electron-electron interactions, Phys. Rev. Lett. **65**, 108 (1990).
[13] D. Pfannkuche and R.R. Gerhardts, Quantum-dot helium: Effects of deviations from a parabolic confinement potential, Phys. Rev. B **44**, 13132 (1991).
[14] W. Kohn, Cyclotron resonance and de Haas–van Alphen oscillations of an interacting electron gas, Phys. Rev. **123**, 1242 (1961).
[15] L. Brey, N.F. Johnson, and B.I. Halperin, Optical and magneto-optical absorption in parabolic quantum wells, Phys. Rev. B **40**, 10647 (1989).
[16] F.M. Peeters, Magneto-optics in parabolic quantum dots, Phys. Rev. B **42**, 1486 (1990).
[17] M.B. Tavernier, E. Anisimovas, F.M. Peeters, B. Szafran, J. Adamowski, and S. Bednarek, Four-electron quantum dot in a magnetic field, Phys. Rev. B **68**, 205305 (2003).
[18] S.-R.E. Yang and A.H. MacDonald, Coupling between edge and bulk in strong-field quantum dots, Phys. Rev. B **66**, 041304 (2002).
[19] S.M. Reimann, M. Koskinen, and M. Manninen, Formation of Wigner molecules in small quantum dots, Phys. Rev. B **62**, 8108 (2000).
[20] B. Szafran, S. Bednarek, J. Adamowski, M.B. Tavernier, E. Anisimovas, and F.M. Peeters, Accuracy of the Hartree–Fock method for Wigner molecules at high magnetic fields, Eur. Phys. J. D **28**, 373 (2004).
[21] M. Ferconi and G. Vignale, Density functional theory of the phase diagram of maximum-density droplets in two-dimensional quantum dots in a magnetic field, Phys. Rev. B **56**, 12108 (1997).
[22] U. De Giovannini, F. Cavaliere, R. Cenni, M. Sassetti, and B. Kramer, Spin-projected unrestricted Hartree–Fock ground states for harmonic quantum dots, Phys. Rev. B **77**, 035325 (2008).
[23] K. Hirose and N.S. Wingreen, Spin-density-functional theory of circular and elliptical quantum dots, Phys. Rev. B **59**, 4604 (1999).

[24] C. Yannouleas and U. Landman, Spontaneous symmetry breaking in single and molecular quantum dots, Phys. Rev. Lett. **82**, 5325 (1999).

[25] S.M. Reimann, M. Koskinen, M. Manninen, and B.R. Mottelson, Quantum dots in magnetic fields: Phase diagram and broken symmetry at the maximum-density-droplet edge, Phys. Rev. Lett. **83**, 3270 (1999).

[26] M.B. Tavernier, E. Anisimovas, and F.M. Peeters, Ground state and vortex structure of the $N = 5$ and $N = 6$ electron quantum dot, Phys. Rev. B **74**, 125305 (2006).

[27] E. Wigner, On the interaction of electrons in metals, Phys. Rev. **46**, 1002 (1934).

[28] C.C. Grimes and G. Adams, Evidence for a liquid-to-crystal phase transition in a classical, two-dimensional sheet of electrons, Phys. Rev. Lett. **42**, 795 (1979).

[29] E. Rousseau, D. Ponarin, L. Hristakos, O. Avenel, E. Varoquaux, and Y. Mukharsky, Addition spectra of Wigner islands of electrons on superfluid helium, Phys. Rev. B **79**, 045406 (2009).

[30] E.Y. Andrei, G. Deville, D.C. Glattli, F.I.B. Williams, E. Paris, and B. Etienne, Observation of a magnetically induced Wigner solid, Phys. Rev. Lett. **60**, 2765 (1988).

[31] T.H. Oosterkamp, J.W. Janssen, L.P. Kouwenhoven, D.G. Austing, T. Honda, and S. Tarucha, Maximum-density droplet and charge redistributions in quantum dots at high magnetic fields, Phys. Rev. Lett. **82**, 2931 (1999).

[32] A. Matulis and E. Anisimovas, A quasiclassical approach to strongly correlated quantum dots in intense magnetic fields, J. Phys. Condens. Matter **17**, 3851 (2005).

[33] E. Anisimovas and A. Matulis, A quasiclassical model of many-electron quantum dots, Lithuanian J. Phys. **45**, 235 (2005).

[34] A. Matulis and F.M. Peeters, Renormalized perturbation series for quantum dots, J. Phys. Condens. Matter **6**, 7751 (1994).

[35] E. Anisimovas and A. Matulis, Energy spectra of few-electron quantum dots, J. Phys. Condens. Matter **10**, 601 (1998).

[36] J.O. Fjærestad, A. Matulis, and K.A. Chao, Perturbation theory of interacting electrons in a quantum dot with hard-wall confinement potential, Physica Scripta **T69**, 138 (1997).

[37] A. Matulis, J.O. Fjærestad and K.A. Chao, Electron interaction in a quantum dot with hard wall confinement potential, Int. J. Mod. Phys. B **11**, 1035 (1997).

[38] A. Gonzalez, B. Partoens, A. Matulis, and F.M. Peeters, Ground-state energy of confined charged bosons in two dimensions, Phys. Rev. B **59**, 1653 (1999).

[39] B. Partoens, A. Matulis, and F.M. Peeters, Two-electron artificial molecule, Phys. Rev. B **59**, 1617 (1999).

[40] B. Partoens, V.A. Schweigert, and F.M. Peeters, Classical double-layer atoms: Artificial molecules, Phys. Rev. Lett. **79**, 3990 (1997).

[41] A. Matulis and F.M. Peeters, Wigner crystallization in the two electron quantum dot, Solid State Commun. **117**, 655 (2001).

[42] E. Anisimovas, A. Matulis, M.B. Tavernier, and F.M. Peeters, Power-law dependence of the angular momentum transition fields in few-electron quantum dots, Phys. Rev. B **69**, 075305 (2004).

[43] E. Anisimovas, M.B. Tavernier, and F.M. Peeters, Electron-vortex separation in quantum dots, Phys. Rev. B **77**, 045327 (2008).

[44] C. Yannouleas and U. Landman, Two-dimensional quantum dots in high magnetic fields: Rotating-electron-molecule versus composite-fermion approach, Phys. Rev. B **68**, 035326 (2003).

[45] M. Büttiker, Y. Imry, and R. Landauer, Josephson behavior in small normal one-dimensional rings, Phys. Lett. A **96**, 365 (1983).

[46] L.P. Levy, G. Dolan, J. Dunsmuir, and H. Bouchiat, Magnetization of mesoscopic copper rings: Evidence for persistent currents, Phys. Rev. Lett. **64**, 2074 (1990).

[47] E. Anisimovas, A. Matulis, and F.M. Peeters, Currents in a many-particle parabolic quantum dot under a strong magnetic field, Phys. Rev. B **70**, 195334 (2004).

[48] A. Matulis and E. Anisimovas, Quantum dot properties in a strong magnetic field, Acta Phys. Pol. A **105**, 529 (2004).

[49] P.A. Maksym, Eckardt frame theory of interacting electrons in quantum dots, Phys. Rev. B **53**, 10871 (1996).

[50] A. Radzvilavičius and E. Anisimovas, Configurational entropy of Wigner clusters, J. Phys. Condens. Matter (provisionally scheduled for February 2011).

[51] W.H. Press, S.A. Teukolsky, W.T. Vetterling, and B.P. Flannery, *Numerical Recipes: the Art of Scientific Computing*, 3rd ed. (Cambridge University Press, Cambridge, 2007).

[52] D.P. Landau and K. Binder, *A Guide to Monte Carlo Simulations in Statistical Physics*, 3rd ed. (Cambridge University Press, Cambridge, 2009).

[53] J.R. Morris, D.M. Deaven, and K.M. Ho, Genetic-algorithm energy minimization for point charges on a sphere, Phys. Rev. B **53**, 1740 (1996).

[54] V.M. Bedanov and F.M. Peeters, Ordering and phase transitions of charged particles in a classical finite two-dimensional system, Phys. Rev. B **49**, 2667 (1994).

[55] C. Henning, K. Fujioka, P. Ludwig, A. Piel, A. Melzer, and M. Bonitz, Existence and vanishing of the breathing mode in strongly correlated finite systems, Phys. Rev. Lett. **101**, 045002 (2008).

[56] A. Matulis, D. Jarema, and E. Anisimovas, A quasiclassical approach to strongly correlated quantum dots, Central Eur. J. Phys. **7**, 704 (2009).

[57] M. Hase, M. Kitajima, A.M. Constantinescu, and H. Petek, The birth of quasiparticles in Si observed in time-frequency space, Nature **426**, 51 (2003).
[58] U. Weiss, *Quantum Dissipative Systems*, Series in Modern Condensed Matter Physics Vol. 13, 3rd ed. (World Scientific, Singapore, 2008).
[59] E. Anisimovas and A. Matulis, Schrödinger-equation formalism for a dissipative quantum system, Phys. Rev. A **75**, 022104 (2007).
[60] A. Matulis and E. Anisimovas, Dissipation in a Schrödinger-equation formalism, Physica E **40**, 1520 (2008).
[61] A. Matulis and E. Anisimovas, Dissipation in a quantum-mechanical system, Opt. Mater. **30**, 730 (2008).
[62] W. Boucher and J. Traschen, Semiclassical physics and quantum fluctuations, Phys. Rev. D **37**, 3522 (1988).
[63] Z.L. Ye and E. Zaremba, Magnetoplasma excitations in anharmonic electron dots, Phys. Rev. B **50**, 17217 (1994).
[64] B. Partoens, A. Matulis, and F.M. Peeters, Magnetoplasma excitations of two vertically coupled dots, Phys. Rev. B **57**, 13039 (1998).
[65] E. Anisimovas and F.M. Peeters, Dynamic response of artificial bipolar molecules, Phys. Rev. B **66**, 075311 (2002).

KVAZIKLASIKINĖ KVANTINIŲ TAŠKŲ TEORIJA

E. Anisimovas [a], A. Matulis [b]

[a] *Vilniaus universitetas, Vilnius, Lietuva*
[b] *Fizinių ir technologijos mokslų centro Puslaidininkių fizikos institutas, Vilnius, Lietuva*

Santrauka

Kvantiniai taškai yra dariniai, kuriuose elektrono judėjimas yra apribotas visomis trimis erdvės kryptimis, o energijos spektras diskretus. Taigi, kvantiniai taškai yra dirbtiniai atomai: valdomų parametrų natūralių atomų analogai. Didelių matmenų (lyginant su efektiniu Boro spinduliu) kvantiniuose taškuose klasikinė kuloninės stūmos energija žymiai viršija kvantinę kinetinę energiją. Elektrostatinės sąveikos santykinę svarbą dar labiau išryškina stiprus taško plokštumai statmenas magnetinis laukas. Todėl, viena vertus, šiuose kvantiniuose taškuose yra stebimi kolektyviniai reiškiniai (Vignerio kristalizacija), antra vertus, jų fizika yra iš esmės klasikinė. Straipsnyje apžvelgiama kvaziklasikinė kvantinių taškų teorija, išplėtota pasinaudojus šiais pastebėjimais. Taikomi klasikiniai metodai leidžia išvengti sudėtingų ir nevaizdžių kvantinių mechaninių skaičiavimų. Klasikiniais metodais gauti rezultatai yra lengvai suprantami ir interpretuojami, o į kvantines pataisas atsižvelgiama kaip į mažus trikdžius. Aptariamas renormalizuotos trikdžių eilutės taikymas energijų spektrams skaičiuoti, struktūrų susidarymas ir virsmai kvantiniuose taškuose, laipsniniai dėsniai, nusakantys kritinių parametrų elgesį, ir disipacija mišriose sistemose, pasižyminčiose klasikinių ir kvantinių laisvės laipsnių sąveika.